Advances in the Theory of Atomic and Molecular Systems
Dynamics, Spectroscopy, Clusters, and Nanostructures
Series: Progress in Theoretical Chemistry and Physics , Vol. 20
Piecuch, P.; Maruani, J.; Delgado-Barrio, G.; Wilson, S. (Eds.)
2010, XII, 300 p., Hardcover
ISBN: 978-90-481-2984-3
Online version available

Usually dispatched between 3 to 5 business days

229,00 €

Table of contents

Influence of the Level of Protonation on the Geometry and the Electronic Structure of Emeraldine Oligomers (*Jasmina Petrova, Julia Romanova, Galia Madjarova, Anela Ivanova, Alia Tadjer, and Natalia Gospodinova*)

Quantum Mechanical Examination of Optical Absorption Spectra of Silver Nanorod Dimers (*Jérémy Vincenot and Christine M. Aikens*)

On the Electronic Spectra of a Molecular Bridge Under Non-Equilibrium Electric Potential Conditions (*Alexander Prociuk and Barry D. Dunietz*)

Quantum Chemical Approach to Interatomic Decay Rates in Clusters

V. Averbukh, P. Kolorenč, K. Gokhberg, and L.S. Cederbaum

Abstract Since their theoretical prediction in 1997, interatomic (intermolecular) Coulombic decay (ICD) and related processes have been in the focus of intensive theoretical and experimental research. The spectacular progress in this direction has been stimulated both by the fundamental importance of the discovered electronic decay phenomena and by the exciting possibility of their practical application, for example, in spectroscopy of interfaces. Interatomic decay phenomena take place in inner-shell-ionized clusters due to electronic correlation between two or more cluster constituents. These processes lead to the decay of inner-shell vacancies by electron emission and often also to the disintegration of the resulting multiple ionized cluster. The primary objective of the theory is, thus, to predict the kinetic energy spectra of the emitted electrons and of the cluster fragments. These spectra are determined by an interplay between the electronic decay process and the nuclear dynamics. Key to the reliable prediction of the observable quantities is the knowledge of the time scale of the interatomic decay. Here we review the recent progress in the development of ab initio quantum chemical methods for the calculation of interatomic decay rates in excited, singly ionized, and doubly ionized systems as well as some of their applications, e.g., to rare gas systems and to endohedral fullerenes.

V. Averbukh (✉)
Max Planck Institute for the Physics of Complex Systems, Nöthnitzer Str. 38, D-01187 Dresden, Germany, e-mail: vitali@mpipks-dresden.mpg.de

P. Kolorenč
Institute of Theoretical Physics, Faculty of Mathematics and Physics, Charles University in Prague, V Holešovičkách 2, 180 00 Prague, Czech Republic, e-mail: kolorenc@mbox.troja.mff.cuni.cz

K. Gokhberg
Theoretische Chemie, Physikalisch-Chemisches Institut, Universität Heidelberg, Im Neuenheimer Feld 229, D-69120 Heidelberg, Germany, e-mail: Kirill.Gokhberg@pci.uni-heidelberg.de

L.S. Cederbaum
Theoretische Chemie, Physikalisch-Chemisches Institut, Universität Heidelberg, Im Neuenheimer Feld 229, D-69120 Heidelberg, Germany, e-mail: Lorenz.Cederbaum@pci.uni-heidelberg.de

P. Piecuch et al. (eds.), *Advances in the Theory of Atomic and Molecular Systems*, Progress in Theoretical Chemistry and Physics 20, DOI 10.1007/978-90-481-2985-0_8,

Keywords: Interatomic Coulombic decay · Ab initio calculations · Inner-shell ionization · Clusters

1 Introduction

The present day knowledge of interatomic (intermolecular) decay mechanisms in clusters encompasses a diversity of distinct physical phenomena, all stemming from interatomic (intermolecular) electronic interaction. In this section we give an overview of the predicted and observed interatomic decay processes.

1.1 Interatomic (Intermolecular) Coulombic Decay: A General Decay Mode of Auger-Inactive Inner-Shell-Ionized States

Core vacancy states of atoms and molecules represent very highly excited states of the corresponding atomic or molecular ions, typically lying above the double or even multiple ionization thresholds. As a result, these states decay by electron emission in a specific type of autoionization process named after its discoverer, Auger [1]. Kinetic energies of the electrons emitted in the course of Auger decay are given by the differences between the bound states of singly and doubly charged species and thus are quantized. This property explains the great spectroscopic value of the Auger electron spectroscopy (AES) [2], as well as its importance for numerous analytical applications, e.g., in surface science (see, for example, Ref. [3]). Auger decay is typically an intraatomic process, only modestly affected by the environment. Usually, such an effect is manifested in the so-called chemical shift of the Auger electron lines (see, for example, Ref. [4]).

In 1997, the authors of the theoretical work [5] took a pioneering approach to the issue of the environment effects on the decay of vacancy states [5]. The question posed by the authors was:

> Can a vacancy decay non-radiatively *only* due to the effect of the environment?

Surprisingly, it turned out that such an environment-mediated decay is not only possible, but also a general phenomenon, typical of relatively low-energy inner-shell vacancies in a wide variety of clusters [5]. In order to get an idea of the new decay process discovered by Cederbaum and co-workers, one can consider the decay of $2s$ vacancy of neon, once in an isolated ion and once in a cluster, e.g., in Ne_n. The $2s^{-1}$ state of the isolated Ne^+ lies below the double ionization threshold of Ne and thus cannot decay by Auger mechanism. As a result, $(2s^{-1})$ Ne^+ decays radiatively on a nanosecond time scale. However, if $(2s^{-1})$ Ne^+ is allowed to interact with an environment, e.g., with other Ne atoms, the situation changes dramatically. Indeed, as shown schematically in Fig. 1 for neon dimer, in a Ne_n cluster, one can consider not only the high-energy $Ne^{2+}Ne_{n-1}$ doubly ionized states, but also the ones of the type $(Ne^+)_2Ne_{n-2}$. The latter states are relatively low in energy due to the separation of the positive charge between two neon atoms. In fact, the charge-separated states

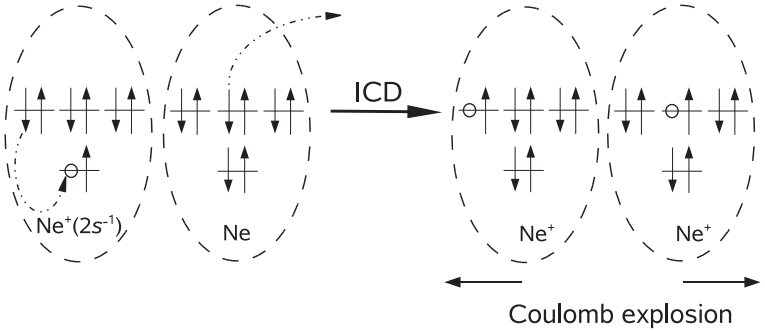

Fig. 1 A schematic representation of the ICD process in Ne dimer. A $2p$ electron of the inner-valence-ionized Ne recombines into the $2s$ vacancy while a $2p$ electron of another Ne is ejected into continuum. The resulting doubly charged cluster decomposes by Coulomb explosion mechanism

lie several electron-volts lower than $(2s^{-1})$ $Ne^{+}Ne_{n-1}$. This leads to a very interesting *interatomic* decay process in which $2p$ electron of the ionized Ne fills the $2s$ vacancy, while $2p$ electron of another Ne atom is ejected into continuum. Since such a process is enabled by the Coulombic interaction between the electrons of the two Ne atoms, it has been called interatomic Coulombic decay (ICD). In a small loosely bound cluster, such as neon dimer, the repulsion between the two charges created by ICD leads to Coulomb explosion of the system [6] (see Ref. [7] for an exception). Under such conditions, the excess energy of the initial vacancy state is partitioned between the outgoing electron and the separating positively charged fragments. Thus, while Auger decay leads to quantized Auger electron energies, ICD in small clusters makes the total of the electron and the cluster fragment energies to be quantized. The kinetic energy of the relative motion of the fragments is often called kinetic energy release (KER).

The last several years have witnessed a series of remarkable advances in the experimental study of ICD. Hergenhahn, Möller, and co-workers have presented the first experimental evidence of ICD by clearly identifying the new process in neon clusters [8]. Dörner, Jahnke, and co-workers have conducted a detailed study of ICD in neon dimer [9] using the cold target recoil ion momentum spectroscopy (COLTRIMS) [10]. They have been able to measure in coincidence both the ICD electrons and the neon ions generated by the Coulomb explosion of $(Ne^{+})_2$. The coincidences detected by Frankfurt group were found to be arranged along the energy conservation line corresponding to the sum of the electron energy and the KER being about 5 eV. Thus, the experiment of Dörner and co-workers constitutes the most detailed direct proof of the ICD. The electron kinetic energy and the KER spectra of Frankfurt group were later confirmed by theoretical calculations [11]. Going back to larger neon clusters, Örwall et al. have estimated the dependence of the ICD lifetime on the neon cluster size by distinguishing between the "bulk" and the "surface" peaks in the ICD electron spectra [12]. These experimental findings were found it to be in a reasonable agreement with earlier theoretical predictions of Santra et al. [13] (see also the more recent theoretical work of Vaval and Cederbaum [14]).

Both theoretical and experimental investigations have established ICD as a highly general and a very efficient decay process. Indeed, ICD is characteristic of vacancy states of van der Waals clusters (see, e.g., Refs. [5, 8]), hydrogen-bonded clusters (see, e.g., Refs. [15, 61]), and even endohedral fullerenes [16]. The ICD lifetimes were found to belong to the range of 1–100 fs [12, 13, 16], many orders of magnitude shorter than those of the competing photon emission process. Thus, ICD is the main decay mode of moderate-energy (Auger-inactive) inner-shell vacancies in clusters. Further studies of ICD are motivated, however, not only by the generality and efficiency of this new physical process, but also by the perspectives of its practical use, for example, in spectroscopy. The very first step in this highly promising direction has been already done by Hergenhahn and co-workers who have shown that the ICD electron spectra can be used in order to identify the Ne/Ar interface [17].

1.2 Beyond ICD of Singly Ionized States

1.2.1 Interatomic Decay in Inner-Shell Excitations

Recently, Barth et al. [18] have addressed the question whether interatomic decay can occur not only in the inner-valence-ionized, but also in the inner-valence-excited states of clusters. They have created Ne $(2s^{-1}3p)$ excitations in Ne_n clusters (n being 70 on average) and detected the electrons emitted due to the (Ne $2s^{-1}3p$)$Ne_{n-1} \rightarrow$ (Ne $2p^{-1}3p$)(Ne^+ $2p^{-1}$)$Ne_{n-2} + e^-$ process. Aoto et al. [19] studied in detail a similar decay phenomenon in neon dimer. This process is related to ICD exactly in the same way in which the resonant Auger effect [20, 21] is related to the regular Auger effect [1, 2]. Consequently, it has been called resonant interatomic Coulombic decay (RICD) [18].

The RICD physics is richer and more involved than the ICD physics due to several reasons. First, the interatomic decay of inner-shell-excited states is accompanied by the intraatomic autoionization, e.g., $(2s^{-1}3p)\text{Ne} \rightarrow (2p^{-1})\text{Ne} + e^-$. Whereas ICD competes only with slow radiative decay, RICD has to compete with a fast non-radiative process. Nevertheless, both experimental [18, 19] and theoretical [22] evidences show that this competition does not lead to a suppression of RICD. Another important difference between ICD and RICD comes from the fact that the inner-valence-excited electron can participate in the RICD process. Exactly as the resonant Auger decay [20, 21], RICD can occur either by *spectator* (*s*RICD) or by *participator* (*p*RICD) mechanism. While the *s*RICD process has been observed experimentally, *p*RICD has yet to be identified in the RICD electron spectra.

Yet another distinction between ICD and RICD has its origin in the higher energy accumulated in the inner-valence-excited states relative to the one of the inner-valence-ionized states. For example, $(2s^{-1}3p)$Ne lies about 45.5 eV above the Ne ground state, whereas $(2s^{-1})$ Ne^+ lies only about 26.9 eV above the Ne^+ ground state. As a result, decay of inner-valence-ionized states can be accompanied by double ionization of the cluster. This can happen according to a variety of mechanisms which have been discussed qualitatively in Ref. [22]. The predicted double ioniza-

tion interatomic processes still await their detailed quantitative study. The essential question is whether the double ionization processes are fast enough to compete with autoionization and *s*RICD.

1.2.2 Auger–ICD Cascade

It is well known that Auger decay of core vacancies often results in highly excited states of the corresponding doubly ionized species. Sometimes, this brings about another stage (or even several stages) of Auger decay, forming what is usually called a decay cascade. Often, however, the excited doubly ionized states created by Auger process are not energetic enough to decay by an intraatomic mechanism. Under such conditions, formation of decay cascade is impossible in isolated species, but can occur in clusters with the second step of the cascade being of the ICD, rather than of the Auger type. The Auger–ICD cascade has been first predicted by Santra and Cederbaum [23] in neon dimer (see also the more recent theoretical work [24]) and has first been observed by Ueda and co-workers [25] in argon dimers (see also the theoretical work [26]).

The Auger–ICD cascade in neon dimer can be represented as $(1s^{-1})\mathrm{Ne}^{+}\mathrm{Ne} \rightarrow (2s^{-1}2p^{-1})\mathrm{Ne}^{2+}\ \mathrm{Ne} + e^{-} \rightarrow (2p^{-2})\mathrm{Ne}^{2+} + \mathrm{Ne}^{+} + e^{-}$. Interestingly, a similar process starting with $2p$ ionization of argon dimer is energetically forbidden: the $3s^{-1}3p^{-1}$ states of Ar^{2+} are not energetic enough to lead to ICD. Observation of Auger–ICD cascade in Ar_2 [25] has been nevertheless possible due to the fact that Auger decay populates not only the $3s^{-1}3p^{-1}$ main states, but also higher-energy satellites having admixture of $3p^{-3}3d$ configurations. More recently, ICD after Auger decay in neon dimer has been extensively studied [27–29]. Experimental work on the Auger–ICD cascade in NeAr is now in progress [30].

Further exploration of the fascinating subject of the interatomic decay phenomena and development of spectroscopic tools on their basis requires intensive theoretical effort to guide the experimental work. Such an effort is hardly possible without efficient, advanced theoretical tools involving both ab initio description of the electron correlation driving the decay and a treatment of the ensuing dynamics of the ionized cluster fragments. The next section gives the theoretical picture of interatomic decay within the Born–Oppenheimer (BO) approximation. Ab initio theory of the interatomic decay widths is presented in some detail for the case of the ICD process in Sect. 3. Sections 4 and 5 are devoted to ab initio theory and computational algorithms for the interatomic decay widths in doubly ionized and inner-shell-excited systems, respectively. Some considerations on the future of the field are summarized in Sect. 6.

2 Born–Oppenheimer Picture of Interatomic Decay

The main objective of the theory of ICD is to enable efficient and reliable calculation of the measurable spectra, i.e., ICD electron kinetic energy spectrum and (where applicable) KER spectrum. The theoretical description is usually given

within Born–Oppenheimer approximation, in which the electronic states are decoupled from nuclear motion and depend only parametrically on the nuclear coordinates. In this picture, the inner-shell ionization and the subsequent ICD process can be visualized as a series of transitions between potential energy surfaces (PESs) belonging to electronic states of different number of electrons (i.e., accompanied by electron emission). These transitions are represented schematically in Fig. 2. Initially, the system is assumed to be in the ground electronic state of the neutral (N-electron) system. The corresponding PESs of loosely bound clusters are characterized by shallow minima (e.g., in meV range for van der Waals systems) and large equilibrium interatomic distances. Photoionization brings the cluster almost instantaneously into inner-shell-ionized (typically, inner-valence-ionized) [$(N-1)$-electron] state, being the intermediate state of the decay. The PES of the singly ionized system is affected by the charge-induced dipole interaction that increases the binding energy and decreases the equilibrium interatomic distances relative to

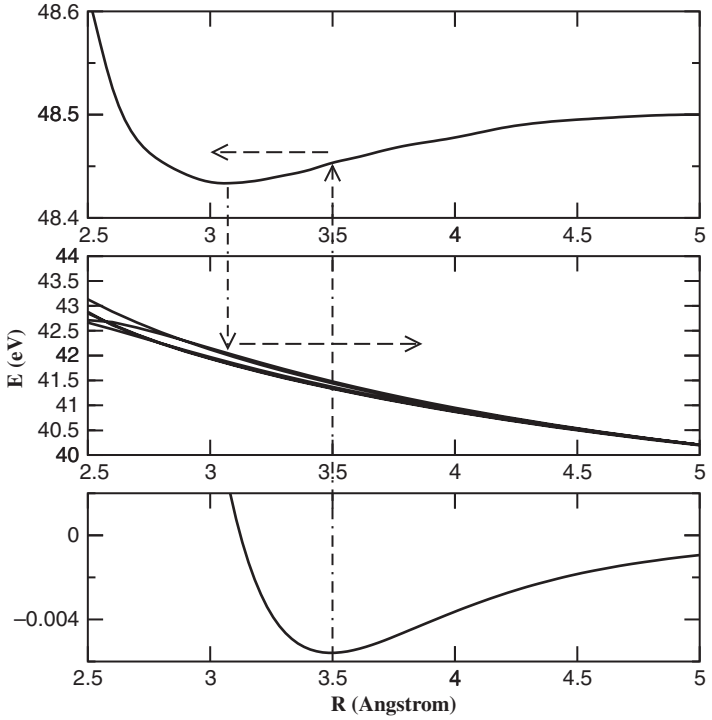

Fig. 2 Schematic representation of ICD process in Born–Oppenheimer picture. PESs of NeAr [33] are used as a representative example. Lower frame: ground-state PES of the neutral diatom (initial state). Upper frame: inner-valence-ionized (intermediate state) PES. Middle frame: doubly ionized (final state) PESs. Transitions between the PESs accompanied by loss of an electron are shown by *dashed–dotted lines*. Directions of motion of nuclear wave packets on intermediate and final state PESs are shown by *dashed lines*

the van der Waals ground state. This means that after landing on the inner-shell-ionized PES, the nuclear wave packet is driven toward shorter internuclear distances. Due to the ICD, the intermediate state has finite lifetime. This means that the nuclear wave packet moving on the intermediate state PES can lose some of its density to the final (doubly ionized) state PESs. The latter are typically dominated by the repulsion between the two positive charges and are often close to the purely Coulombic repulsive shape. The geometry at which the decay occurred determines the partition of energy between the outgoing electron and the repelling fragments.

The above qualitative picture has its full formal analog in the so-called time-dependent formulation of the theory of nuclear dynamics of electronic decay processes. This theory is given in some detail in Ref. [11] and in references therein. Here we will consider only its few principal points. Let us denote the nuclear wave packets for the initial (i), intermediate (d), and final (f) electronic states as Ψ_i, Ψ_d, and Ψ_m^f, respectively, where the index m accounts for the possibility that there are several final electronic states (see Fig. 1). We assume that the electric field used in order to ionize the initial state is weak enough (weak-field approximation) and describes the coupling between the intermediate and the final states of the decay in the so-called local approximation [11]. Under these approximations, the nuclear wave packets obey the following set of coupled differential equations:

$$\begin{aligned}
\hbar\frac{\partial}{\partial t}|\Psi_i(R,t)\rangle &= \hat{H}_i(R)|\Psi_i(R,t)\rangle,\\
\hbar\frac{\partial}{\partial t}|\Psi_d(R,t)\rangle &= \hat{F}(R,t)|\Psi_i(R,t)\rangle + \hat{\mathcal{H}}_d(R)|\Psi_d(R,t)\rangle,\\
\hbar\frac{\partial}{\partial t}|\Psi_m^f(R,\varepsilon,t)\rangle &= \hat{W}_m(R,\varepsilon)|\Psi_d(R,t)\rangle + (\hat{H}_m^f(R)+\varepsilon)|\Psi_m^f(R,\varepsilon,t)\rangle\,,
\end{aligned} \tag{1}$$

where ε is the energy of the electron emitted during ICD.

The Hamilton operators for the nuclear motion in the initial and final electronic states in Eq. (1) are defined as $\hat{H}_i = \hat{T}_N + \hat{V}_i$ and $\hat{H}_m^f = \hat{T}_N + \hat{V}_m^f$, where $\hat{T}_N$ is the nuclear kinetic energy and $\hat{V}_i$ and $\hat{V}_m^f$ are the initial and final state PESs, respectively. The effective Hamilton operator governing the intermediate state dynamics has to account for the fact that the intermediate state is an electronic resonance. Within the local approximation, this is done by lending the intermediate state Hamiltonian a non-Hermitian character:

$$\hat{\mathcal{H}}_d(R) = \hat{T}_N(R) + \hat{V}_d(R) - i\hat{\Gamma}(R)/2\,, \tag{2}$$

where $\hat{V}_d(R)$ is the intermediate state PES and $\hat{\Gamma}(R)$ is the total decay width.

The coupling operators $\hat{F}$ and $\hat{W}_m$ describe the excitation from the initial to the intermediate electronic state and the coupling of the latter to the mth final state, respectively. Since we assume the inner-shell ionization to occur instantaneously, $\hat{F}$ can be taken to be R independent and simply a δ-function in time. The $\hat{W}_m$

operators describe the coupling of the intermediate state to the different final states. Within the local approximation, they are energy independent and are related to the corresponding partial decay widths: $\Gamma_m(R) = 2\pi |\hat{W}_m(R)|^2$.

As shown, e.g., in Ref. [11, 31, 32], all the information concerning the decay spectrum can be derived from the knowledge of the final nuclear wave packets. Indeed, at sufficiently large time (i.e., when the decay is complete and the norm of all the intermediate wave packet is zero), only the final states are populated and thus carry all the spectroscopic information of interest. In particular, the decay spectrum as a function of the emitted electron energy ε is given by [11, 31]

$$\sigma(\varepsilon) = \lim_{t\to\infty} \sum_m \sigma_m(\varepsilon, t) = \lim_{t\to\infty} \sum_m \langle \Psi_m^f(R, \varepsilon, t) | \Psi_m^f(R, \varepsilon, t) \rangle \,. \tag{3}$$

Equations in (1) show clearly that the shape of the spectrum (3) is determined by two competing time scales: that of the nuclear wave packet motion on the intermediate PES and that of the interatomic decay. If the decay is fast relative to the nuclear motion, the ICD occurs around the equilibrium geometry of the neutral (see Ref. [33] for a recent example of this kind). If, on the other hand, decay is slow on the scale of the nuclear wave packet evolution, ICD occurs within a wide range of geometries. In the latter case, various contributions are expected to interfere resulting in a complex pattern of $\sigma(E)$ [see Eq. (3)]. Thus, an accurate computation of the ICD width of the intermediate state is crucial for a reliable prediction of the ICD spectra.

3 ICD Widths by Fano–ADC–Stieltjes Method

Calculation of ICD widths can be achieved within one of the two main theoretical approaches. One of them relies on the introduction of complex absorbing potential (CAP) [34, 35] into the $(N-1)$-electron Hamiltonian [36] (see Refs. [37] on the relation between the CAP method and the method of exterior complex scaling). The decay widths are then given by the imaginary parts of those eigenvalues of the resulting non-Hermitian Hamiltonian [$E = \Re(E) - i\Gamma/2$] that are stationary with respect to the non-physical CAP parameters. The $(N-1)$-electron Hamiltonian can be represented using a variety of ab initio techniques, such as, for example, configuration interaction (CI) or algebraic diagrammatic construction (ADC) [38] within the intermediate state representation (ISR) [39]. The application of the CAP–CI method to calculate ICD widths has been reviewed in detail in Ref. [40]. More recently, CAP–ADC method [40] based on the ADC–ISR representation of the many-electron Hamiltonian has been developed [41–43] and applied to ICD [14]. An alternative ab initio approach to calculate the interatomic decay widths on which we would like to concentrate here [44] relies on Fano theory of resonances [45], ADC–ISR representation of the many-electron wave functions [39], and Stieltjes imaging technique [46].

3.1 ICD Within Fano Theory of Resonances

Fano theory of resonances [45] as well as its generalized version [47, 48] developed for the description of Auger decay widths represents the wave function Ψ_E at some energy E above threshold as a superposition of bound-like (Φ) and continuum-like (χ_ε) components, which can be thought of as the initial and final states of the decay:

$$\Psi_{\alpha,E} = a_\alpha(E)\Phi + \sum_{\beta=1}^{N_c} \int C_{\beta,\alpha}(E,\varepsilon)\,\chi_{\beta,\varepsilon}\,d\varepsilon\,, \tag{4}$$

where the index β runs over the N_c possible decay channels. In the specific case of interatomic (intermolecular) decay in clusters, the bound part of the wave function, Φ, corresponds to the singly ionized state, typically created by the inner-valence ionization of one of the cluster subunits. The state Φ is characterized by the mean energy

$$E_\Phi = \langle \Phi | H | \Phi \rangle\,, \tag{5}$$

H being the full Hamiltonian of the system. The N_c decay channels in Eq. (4) are defined by the doubly ionized states of the cluster characterized by the energies $E_\beta < E$, $\beta = 1, \ldots, N_c$, i.e., by the energetically accessible final states of the interatomic (intermolecular) decay. The continuum functions corresponding to the decay channels are assumed to diagonalize the Hamiltonian to a good approximation:

$$\langle \chi_{\beta',\varepsilon'} | H - E | \chi_{\beta,\varepsilon} \rangle \approx (E_\beta + \varepsilon - E)\,\delta_{\beta',\beta}\,\delta(E_{\beta'} + \varepsilon' - E_\beta - \varepsilon)\,. \tag{6}$$

Using the assumption of uncoupled continuum functions, Fano theory provides an analytic expression for the evaluation of the decay width:

$$\Gamma = \sum_{\beta=1}^{N_c} \Gamma_\beta = 2\pi \sum_{\beta=1}^{N_c} \left| M_\beta(E_r, \varepsilon_\beta) \right|^2\,, \quad M_\beta(E,\varepsilon) = \langle \Phi | H - E | \chi_{\beta,\varepsilon} \rangle\,, \tag{7}$$

where E_r is the real energy of the decaying state, $E_r \approx E_\Phi = \langle \Phi | H | \Phi \rangle$ and ε_β is the asymptotic kinetic energy of the ejected electron for the decay channel β, $E_r = E_\beta + \varepsilon_\beta$.

3.2 Initial and Final States of the ICD by Algebraic Diagrammatic Construction in the Framework of the Intermediate State Representation

For the result (7) to be applicable to the computation of the interatomic decay rates, one has to provide sensible approximations for the multi-electron bound (Φ) and continuum ($\chi_{\beta,\varepsilon}$) wave functions. In our case, these are wave functions of a singly ionized N-electron cluster, i.e., $(N-1)$-electron states. Such states can be conveniently constructed using the single ionization ADC technique. The ADC methodology has been originally developed within the Green's function formalism [38]. Here, however, we would like to briefly review the single ionization ADC from a different standpoint, using the intermediate state representation (ISR) as proposed by Schirmer et al. [39].

Consider the Hartree–Fock (HF) ground state of the N-electron neutral cluster, Φ_0^N. One can form a complete orthonormal set of the $(N-1)$-electron basis functions, $\Phi_J^{(N-1)}$, applying the so-called physical excitation operators, $\{\hat{C}_J\}$, to the HF ground state:

$$\begin{aligned} \Phi_J^{(N-1)} &= \hat{C}_J \Phi_0^N, \\ \{\hat{C}_J\} &\equiv \{c_i;\, c_a^\dagger c_i c_j, i<j;\, c_a^\dagger c_b^\dagger c_i c_j c_k, a<b, i<j<k;\, \ldots\}, \end{aligned} \tag{8}$$

where c_i and $c_a^\dagger$ are annihilation and creation operators, respectively, the subscripts $i, j, k, \ldots$ relate to the occupied spin orbitals, and the subscripts $a, b, c, \ldots$ relate to the unoccupied spin orbitals. The basis set (8) is used in the familiar CI expansion of the wave function. This expansion, once truncated after some specific excitation class $[J]$, possesses such important drawbacks as slow convergence and lack of size consistency. The ADC method overcomes these drawbacks by using a more complicated basis for the expansion of the $(N-1)$-electron wave functions. The idea is to apply the physical excitation operators, $\{\hat{C}_J\}$, to the perturbation theoretically corrected or "correlated" ground state of the neutral system,

$$\begin{aligned} \Psi_J^0 &= \hat{C}_J \Psi_0^N \\ \Psi_0^N &= \Phi_0^N + \Psi_0^{(1)} + \Psi_0^{(2)} + \Psi_0^{(3)} + \cdots, \end{aligned} \tag{9}$$

where $\Psi_0^{(n)}$ is the nth-order correction to the HF ground state obtained by the standard many-body perturbation theory (see, e.g., Ref. [49]). Unfortunately, the resulting correlated excited states (CESs), Ψ_J^0, are not orthonormal. ADC takes care of this problem by orthonormalizing them in two steps to obtain the so-called intermediate states, $\tilde{\Psi}_J$. First, Gram–Schmidt orthogonalization *between the excitation classes* is performed to obtain the "precursor" states

$$\Psi_J^{\#} = \Psi_J^0 - \sum_{[K]}^{K<[J]} \langle \tilde{\Psi}_K | \Psi_J^0 \rangle \tilde{\Psi}_K \,, \tag{10}$$

i.e., the functions belonging to the higher [e.g., two-hole, one-particle (2h1p) or $[J] = 2$] excitation class are made orthogonal to those of all the lower [in this case, only one-hole (1h) or $[K] = 1$] excitation classes. Second, the precursor states are orthonormalized symmetrically *inside each excitation class*:

$$\tilde{\Psi}_J = \sum_{[J']=[J]}^{J'} \left(\underline{\underline{\rho}}^{\#-\frac{1}{2}}\right)_{J',J} \tilde{\Psi}_{J'} \,, \qquad \left(\underline{\underline{\rho}}^{\#}\right)_{J',J} = \langle \Psi_{J'}^{\#} | \Psi_J^{\#} \rangle, \tag{11}$$

where $\left(\underline{\underline{\rho}}^{\#}\right)_{J',J}$ is the overlap matrix of the precursor states belonging to the same excitation class. The above two-step procedure can be applied iteratively, noting that the correlated excited states of the lowest (1h) excitation class are by definition also the precursor states.

Any state of the $(N-1)$-electron system can be represented using the orthonormal basis of the intermediate states:

$$\Psi_q^{(N-1)} = \sum_i \sum_{[J]=i} Y_{q,J} \tilde{\Psi}_J \,. \tag{12}$$

The expansion coefficients, Y_J, are obtained by the diagonalization of the Hamiltonian matrix constructed in the basis of the intermediate states. It is a crucial feature of the ADC approach that the Hamiltonian matrix elements of the type $\langle \tilde{\Psi}_J | H | \tilde{\Psi}_J \rangle$ can be expressed analytically via the orbital energies and the electron repulsion integrals if one performs the orthonormalization procedure of Eqs. (10, 11) approximately and consistently with the order of the many-body perturbation theory which is used for the construction of the correlated ground state [see Eq. (9)]. Moreover, it can be shown [39] that truncation of the expansion (12) after the excitation class $[J] = m$ introduces an error of the order of $2m$, which should be compared to $m + 1$ for the slower-converging CI expansion. The accuracy of the expansion in excitation classes (12) should be, of course, consistent with that of the perturbation-theoretical series for the correlated ground state (9). Thus, the order, n, at which the perturbation-theoretical expansion (9) is truncated is the single parameter defining the level of the ADC approximation. For this reason, ADC schemes of various quality are usually denoted as ADC(n), $n = 2, 3, 4, ...$, in full analogy with the well-known MP2, MP3, MP4, ... perturbation-theoretical techniques for the ground state of the neutral system. The ADC(2) scheme for singly ionized states describes the many-electron wave functions in the basis of 1h and 2h1p intermediate states treating the coupling between the 1h states and between 1h states and 2h1p states in the second and in the first order, respectively. ADC(2) approximation neglects the coupling between the different 2h1p basis functions. The extended ADC(2) scheme [ADC(2)x] takes into account the coupling between the 2h1p states in the

first order (i.e., on CI level). The third-order ADC(3) scheme, while still confined to the basis of 1h and 2h1p intermediate states, treats the coupling between the 1h states and between 1h states and 2h1p states in the third and in the second order, respectively. A detailed description of the single ionization ADC(2) and ADC(3) schemes, including the expressions for the Hamiltonian matrix elements can be found in Ref. [50]. The proof of the size consistency of the ADC(n) schemes has been given in Ref. [39]. The main limitation of the existing ADC(n) schemes is that they are applicable to ionized and/or excited states of closed shell systems only. Here we are interested in applying ADC to the interatomic (intermolecular) decay in ionized van der Waals and hydrogen-bonded clusters, all of which satisfy this requirement.

Our main purpose is to demonstrate that the ADC(n) schemes can be used for the ab initio calculations of the decay rates within Fano formalism. To this end, we need to show that both bound (Φ) and continuum ($\chi_{\beta,\varepsilon}$) components of the $(N-1)$-electron wave function describing the decay process [see Eq. (4)] can be approximated by the expansion in the basis of the intermediate states (12). Suppose, a vacancy residing on the subunit A of a weakly bound cluster can decay by one of the interatomic (intermolecular) mechanisms, but cannot decay non-radiatively if created in the isolated species A. Clearly, the final state of such a decay will be characterized by two vacancies, one or both of them residing on another cluster subunit. Thus, in order to construct the ADC(n) approximation for the bound part, Φ, one can restrict the physical excitation operators of the higher excitation classes to such where all the holes reside on the subunit A only:

$$\Psi_J^0 = \hat{C}_J \Psi_0^N, \tag{13}$$

$$\{\hat{C}_J\} \equiv \{c_i;\, c_a^\dagger c_i c_j, i<j, \varphi_{i,j} \in A; c_a^\dagger c_b^\dagger c_i c_j c_k, a<b, i<j<k, \varphi_{i,j,k} \in A; \ldots\},$$

where $\varphi_i \in A$ is an occupied spin orbital of the neutral cluster localized on the subunit A. In this way, the intraatomic (intramolecular) relaxation and correlation effects inside the subunit A are taken into account, whereas any kind of interatomic decay cannot be described due to the restriction imposed on the holes. Upon the completion of the selection process, one can construct and diagonalize the Hamiltonian in the basis of the restricted set of the intermediate states using the standard methods. The ADC(n) state approximating the Φ component can be identified, for example, as the one possessing the maximal overlap with the cluster orbital representing the initial vacancy. Since no configurations corresponding to the open decay channels were used in the ADC–ISR expansion for the bound-like component, Φ will be one of the lowest energy eigenvectors of the ADC Hamiltonian. Therefore, a highly efficient Davidson diagonalization technique [51] can be used to diagonalize the matrix.

Once the ADC(n) approximation for the bound component of the wave function has been provided, the remaining task is to construct the approximate continuum components, $\chi_{\beta,\varepsilon}$, describing the possible final states of the interatomic (intermolecular) decay. Such states are naturally found among the ADC(n) eigenstates of the

2h1p character:

$$\chi_{\beta,\varepsilon} \sim \Psi_q^{2\mathrm{h1p}} = \sum_i \sum_{[J]=i} Y_{q,J} \tilde{\Psi}_J \,, \quad 1 - \sum_{[J]=2} |Y_{q,J}|^2 \ll 1 \,. \tag{14}$$

The $\Psi_q^{2\mathrm{h1p}}$ functions can be constructed without any restriction of the kind of (13) being imposed on the physical excitation operators. It is, thus, possible that some intermediate states contribute both to Φ and to $\Psi_q^{2\mathrm{h1p}}$ expansions, leading to $\langle \Phi | \Psi_q^{2\mathrm{h1p}} \rangle \neq 0$. This does not lead to complications as the Fano formalism that we are using does not assume the orthogonality of the bound and the continuum components.

Application of the selection scheme described above is not straightforward in the case of symmetric clusters, e.g., those in which the ionized inner-shell orbital is delocalized due to inversion symmetry. As has been shown in Ref. [52], this difficulty can be circumvented by using the appropriate linear combinations of the "standard" configurations.

3.3 Stieltjes Imaging Technique for Calculation of the Interatomic Decay Widths

Despite the ability of ADC(n) to produce 2h1p-like wave functions in the continuum region of the spectrum , there still exists a series of major difficulties in associating these ADC(n) eigenstates with the approximate continuum states of Fano theory. All these difficulties stem from the fact that the ADC(n) calculations, and ab initio quantum chemical calculations in general, are routinely performed using the $\mathcal{L}^2$ bases, usually the Gaussian ones. As a result, the $\mathcal{L}^2$ and not the scattering boundary conditions are imposed and the $\Psi_q^{2\mathrm{h1p}}$ functions are not properly normalized:

$$\langle \Psi_q^{2\mathrm{h1p}} | \Psi_{q'}^{2\mathrm{h1p}} \rangle = \delta_{q,q'} \tag{15}$$

[compare to Eq. (6)]. Moreover, the corresponding eigenenergies, $E_q^{2\mathrm{h1p}}$, are discrete and are not expected to fulfill the energy conservation relation for the non-radiative decay, $E_q^{2\mathrm{h1p}} = E_\Phi$, except by a coincidence. Finally, it is not possible to define rigorously to which decay channel such or another $\Psi_q^{2\mathrm{h1p}}$ state belongs. Indeed, the scattering boundary conditions corresponding to the outgoing electron of the kinetic energy ε_β are not imposed on the $\mathcal{L}^2$ $\Psi_q^{2\mathrm{h1p}}$ function, neither is it derived from an $(N-2)$-electron state of a well-defined energy E_β.

In order to deal with the above complications, one should reconsider the relation (7) for the total decay rate and adapt it to the limitations imposed by the $\mathcal{L}^2$ character of the final state wave functions. To this end, let us rewrite Eq. (7) as following:

$$\Gamma = 2\pi \sum_{\beta=1}^{N_c} \langle \Phi | H - E_r | \chi_{\beta,\varepsilon_\beta} \rangle \langle \chi_{\beta,\varepsilon_\beta} | H - E_r | \Phi \rangle \,. \tag{16}$$

It is easily noticed that the $\chi_{\beta,\varepsilon_\beta}$ functions define an N_c-dimensional space at the resonance energy, in which they act as basis vectors. If the objective is the calculation of the total width only, one can make also any other choice of the basis in this N_c-dimensional space,

$$\sum_{\beta=1}^{N_c} |\chi_{\beta,\varepsilon_\beta}\rangle\langle\chi_{\beta,\varepsilon_\beta}| = \sum_{\beta=1}^{N_c} |\chi'_\beta\rangle\langle\chi'_\beta|, \tag{17}$$

where $\{\chi_{\beta,\varepsilon_\beta}\}$ and $\{\chi'_\beta\}$ basis sets are related by a unitary transformation. This shows that the 2h1p states, Ψ_q^{2h1p}, do not have to correspond directly to the open decay channels in order to be used in the calculation of the total (but not partial!) decay width.

The remaining gap between the $\mathcal{L}^2$ ADC(n) eigenstates and the true continuum functions appearing in Eq. (7) can be bridged in the following way. The expression (7) relates the total decay width to the matrix elements coupling the bound and the continuum components of the wave function, $\langle \Phi | H - E_r | \chi_{\beta,\varepsilon_\beta} \rangle$. The bound wave function component, Φ, is effectively zero outside some region in space which we will call here the "interaction region." The interaction region roughly defines the dimensions of the system in which the decay process occurs and is spanned by $\mathcal{L}^2$ basis used for the construction of Φ. The continuum components, $\chi_{\beta,\varepsilon_\beta}$, are on the other hand non-zero even at the infinite distance from the cluster. It is clear that the Hamiltonian matrix element between the two components has a contribution only from the interaction region. One can, thus, substitute the continuum components in Eq. (7) by the approximate ones, $\tilde{\chi}_{\beta,\varepsilon_\beta}$, which are equal to the true continuum components within the interaction region and go to zero (e.g., as Gaussians) outside the interaction region. Consequently, it is possible to use $\mathcal{L}^2$ approximations in the true continuum components, such as Ψ_q^{2h1p}, in the total widths calculation, provided that the $\mathcal{L}^2$ functions are (i) renormalized, such that they are equal to the continuum wave functions inside the interaction region and (ii) interpolated in energy, such that they satisfy the energy conservation, $E_q^{\mathrm{2h1p}} = E_\Phi$. Both of these goals can be achieved using the procedure known as Stieltjes imaging. This technique has been introduced by Langhoff in the context of calculation of photoionization cross-section using $\mathcal{L}^2$ wave functions and later generalized to the decay rate evaluation by Hazi [46]. Both mathematical foundations and the implementation algorithms of Stieltjes imaging have been repeatedly described in the literature. Here we will only note that the renormalization of the so-called pseudospectrum of the discrete $\mathcal{L}^2$ states possessing energies in the continuum region of the true spectrum can be achieved using the fact that the spectral moments of the quantities of the type of (7) calculated using the pseudospectrum are good approximations to the spectral moments constructed using the true continuum. In our case, this leads to

$$\sum_{\beta} \int E^k \left| \langle \Phi | H - E_r | \chi_{\beta,\varepsilon_\beta} \rangle \right|^2 dE \approx \sum_{q} \left(E_q^{2\mathrm{h1p}} \right)^k \left| \langle \Phi | H - E_r | \Psi_q^{2\mathrm{h1p}} \rangle \right|^2 . \quad (18)$$

The property (18) allows one to use the techniques of moment theory in order to obtain the correct matrix element of the kind of (7) interpolated to the needed value of the continuum state energy. This can be done through a series of consecutive approximations of increasing order, n_S. The more spectral moments one can reliably calculate using the pseudospectrum, the higher is the maximal possible value of n_S and with it, the quality of the final result. A reliable calculation of the spectral moments, in turn, requires a sufficient density of the pseudospectrum states throughout the energy range contributing to the sum (18). This density can be controlled by the choice of the $\mathcal{L}^2$ basis. In the present work, we use the computationally efficient implementation of Stieltjes imaging described in detail by Müller-Plathe and Diercksen [53].

As we have noted above, $\mathcal{L}^2$ methods, such as Stieltjes imaging, do not allow one to formulate a rigorous procedure for the calculation of the *partial* widths. Such a rigorous calculation must involve the true degenerate continuum functions corresponding to the various decay channels. Despite the fact that these functions are not available within the framework of the method used in this work, it is still possible to estimate ICD partial widths using Stieltjes imaging technique [44] by an ad hoc procedure suggested in Ref. [54].

Equation (18) implies that one has to know the *full* discretized spectrum of the Hamiltonian in order to reproduce the spectral moments required in the Stieltjes imaging procedure. It has been realized very early that such a requirement can make the technique inapplicable for large systems in high-quality $\mathcal{L}^2$ basis sets [55]. Very recently, we have proposed a method to overcome the full diagonalization bottleneck of the Stieltjes imaging [56] by using the block Lanczos pseudospectrum [57] much smaller than the Hamiltonian matrix dimension. This technique has been applied successfully to the calculation of the total photoionization cross-section of benzene within the ADC(2) scheme explicitly taking into account single and double electronic excitations [56]. Generalization of the Stieltjes–Lanczos method to the calculation of decay widths is currently being developed by the authors.

3.4 Selected Applications of the Fano–ADC–Stieltjes Method to Interatomic Decay Widths in Clusters

Interatomic decay widths as functions of cluster geometry are not only an essential input for simulations of ICD electron spectra [11, 33], but are also very interesting physical quantities in their own right. The magnitude and the functional form of $\Gamma(R)$ can tell us a lot about physics of interatomic decay. For instance, at large distances, the ICD width can be shown to follow an inverse power law, in most cases $\Gamma_{\mathrm{ICD}}(R) \propto R^{-6}$ [13, 58, 61]. This asymptotic behavior of the decay width can be

explained by a physically appealing virtual photon transfer model which represents the decay process as an emission of a virtual photon by the inner-shell-ionized atom followed by its absorption by a neighboring neutral. The virtual photon transfer model neglects the overlap between the atomic orbitals of the atoms participating in the interatomic process and thus its validity around the equilibrium geometry of the neutral cluster was a subject of debate (see, e.g. Ref. [59]). Using the Fano–ADC–Stieltjes ab initio approach of Sects. 3.1,3.2, 3.3, we have been able to show that the orbital overlap effect leads to a dramatic enhancement of ICD widths in rare gas–alkaline earth diatoms [44, 61] (see Fig. 3).

The discovery of the overlap effect on the ICD rates led us to ask the question of what kind of chemical environment leads to highest possible ICD rates retaining the clear-cut interatomic nature of the process. It has been realized quite early [13] that higher ICD rates are favored by environments with the highest possible number of nearest neighbors. In large neon clusters, for example, a "bulk" $2s$ vacancy would decay faster than the "surface" one [12]. It turns out, though, that even the "bulk" neon ICD rates can be outmatched by interatomic decay in a very interesting group of chemical compounds called endohedral fullerene complexes, e.g., in $Ne@C_{60}$ [16]. Indeed, in $(2s^{-1})$ $Ne^{+}@C_{60}$, the inner-valence-ionized Ne has as many as 60 nearest neighbors to interact with (see Fig. 4), which leads to as many as several hundreds of ICD channels. As a result, the lifetime of $(2s^{-1})$ $Ne^{+}@C_{60}$ is only about 2 fs, in fact shorter than Auger lifetime of isolated core-ionized neon atom [16]. The ultrafast character of ICD is not the only unique feature of interatomic decay

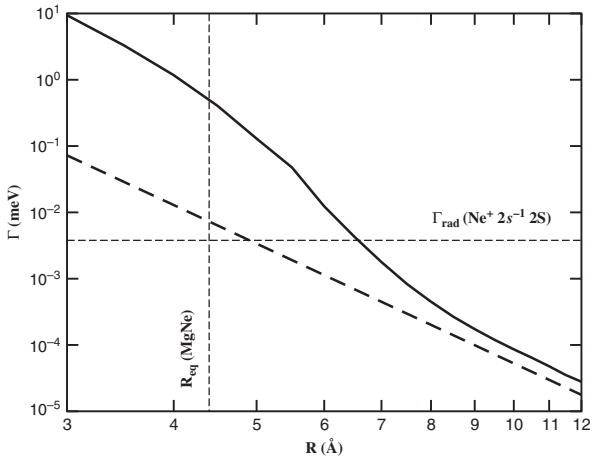

Fig. 3 Doubly logarithmic plot of the total non-radiative decay width of Ne $2s$ vacancy in MgNe cluster as a function of internuclear separation. *Full line*–ADC(2e) result; *dashed line* – virtual photon transfer prediction ([61]) for ICD width. Radiative width of the $2s$ vacancy in free neon atom [60] and the equilibrium distance of MgNe in the ground state are shown by *horizontal* and *vertical dashed lines*, respectively

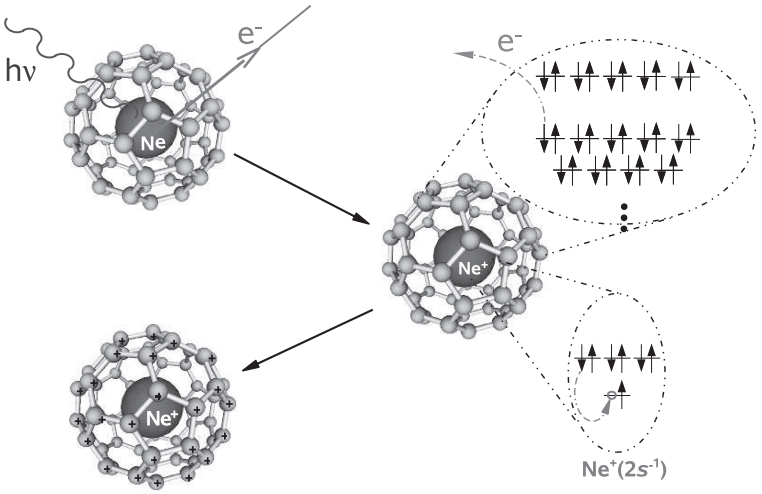

Fig. 4 A schematic drawing of the ICD process in $(2s^{-1})$ Ne@C_{60}: a photon causes inner-valence ionization of the endohedral Ne atom, an outer-valence electron of Ne recombines into the 2*s* vacancy with the released energy being utilized for fullerene ionization

in endohedral fullerenes. A detailed consideration of the possible decay pathways reveals that the relatively low multiple ionization energies of the fullerenes give rise to a number of intriguing new processes, such as double ICD (DICD) (being interatomic analog of double Auger decay [62]), double electron transfer-mediated decay (DETMD), and a two-step cascade of interatomic decay [16]. A combination of ultrafast ICD with the rich pattern of the possible decay channels makes endohedral fullerenes particularly attractive for future theoretical and experimental studies.

4 ICD in Doubly Ionized Clusters

As pointed out in Sect. 1, Auger decay of core vacancies often produces highly excited states of the corresponding doubly ionized species which can, in full analogy with the case of single inner-valence vacancy, undergo interatomic (intermolecular) decay of the ICD type in clusters. Despite the recent progress in the experimental investigation of ICD following Auger decay [25, 27–29, 63], the theoretical description of the phenomenon is much less advanced than that of ICD in single ionized clusters, mainly due to unavailability of accurate data on the interatomic decay widths. However, the success of the Fano–ADC–Stieltjes method, described in Section 3, motivated extension of the approach to the description of the interatomic decay of excited doubly ionized states in clusters [64].

4.1 Fano–ADC–Stieltjes Method for Interatomic Decay Widths in $(N-2)$-Electron Systems

Most computational aspects of the method are fully analogous to the single vacancy case and will not be repeated here. Instead, we will focus only on the few points of difference. Obviously, the principal difference is that the wave function Ψ_E of Eq. (4) represents now doubly ionized ($N-2$-electron) cluster. Therefore, double ionization ADC technique has to be used to construct the bound (Φ) and continuum ($\chi_{\beta,\varepsilon}$) ($N-2$)-electron states. Suitable ADC scheme for the pp-propagator has been derived by Schirmer and Barth [65]. To describe the bound component (Φ, initial state of the decay) of the wave function Ψ_E within the ADC(n) approach, it is necessary to restrict the physical excitation operators generating the CESs Ψ_J^0 (and, in turn, the intermediate states $\tilde{\Psi}_J$) in such a way that open channels of the interatomic decay are not included in the resulting basis.

The intraatomic nature of the Auger decay makes it possible to follow similar strategy as in Sect. 3.2, based on the spatial localization properties of the occupied spin orbitals. Indeed, the initial state of the decay is characterized by two vacancies being localized on a single cluster constituent A, while in the triply ionized final states of Auger–ICD cascade, one or more vacancies reside on another cluster subunit. Therefore, in analogy with Eq. (13), the CESs for the initial state expansion are generated with the restriction that all the holes reside on the subunit A only:

$$\begin{aligned} \Psi_J^0 &= \hat{C}_J \Psi_0^N, \\ \{\hat{C}_J\} &\equiv \{c_i c_j, i<j, \varphi_{i,j} \in A;\, c_a^\dagger c_i c_j c_k, i<j<k, \varphi_{i,j,k} \in A;\, \ldots\}, \end{aligned} \tag{19}$$

where $\varphi_i \in A$ is an occupied spin orbital of the neutral cluster localized on the subunit A. Note that we are now working with two-hole (2h, $J=1$), three-hole, one-particle (3h1p, $J=2$), …excitation classes. Upon diagonalization of the Hamiltonian constructed in the restricted basis of intermediate states generated from the CESs of Eq. (19), the approximation to the initial state is identified as the eigenstate of the desired symmetry with the largest overlap with the 2h configuration describing the initial two vacancies. The approximate continuum components, $\chi_{\beta\varepsilon}$, corresponding to the possible final states of the interatomic decay, are obtained in a separate ADC(n) calculation as the eigenstates of the 3h1p character:

$$\chi_{\beta,\varepsilon} \sim \Psi_q^{3\mathrm{h1p}} = \sum_i \sum_{[J]=i} Y_{q,J} \tilde{\Psi}_J\,, \quad 1 - \sum_{[J]=2} |Y_{q,J}|^2 \ll 1\,. \tag{20}$$

Once the ADC(n) approximations for the bound and continuum components of the wave function (4) are constructed, one can use the Stieltjes imaging procedure of Sect. 3.3 to renormalize the matrix elements computed with the $\mathcal{L}^2$ wave functions, $\Psi_q^{3\mathrm{h1p}}$, and interpolate them in energy as necessary for the computation of the decay widths.

4.2 ICD After Auger Decay in Rare Gas–Alkaline Earth Clusters

To demonstrate the similarities and differences between ICD in singly and doubly ionized clusters, let us investigate the non-radiative decay widths of doubly ionized $Ne^{2+}(2s^{-1}2p^{-1})$ in MgNe diatomic. In the first order of perturbation theory picture, the decay process proceeds in the same way as ICD of the single Ne $2s$ vacancy, since the initial Ne $2p$ vacancy is only a spectator. Higher orders of perturbation theory involve also pathways in which the initial Ne $2p$ vacancy participates actively, but partial width analysis shows that these processes account only for about 5% of the total decay width. The qualitative similarity of the two decay processes is confirmed in Fig. 5, which shows the total non-radiative decay widths of different symmetries of $MgNe^{2+}(2s^{-1}2p^{-1})$ as functions of internuclear distance R. The decay width of $MgNe^{+}(2s^{-1})$ is shown as the full line for reference. At large distances all the widths follow the $\Gamma(R) \propto R^{-6}$ law, predicted by the virtual photon model for dipole–dipole interatomic decay processes. At smaller distances around the equilibrium geometry the overlap between atomic orbitals of the two involved atoms leads to significant enhancement of ICD widths as in the case of ICD of singly ionized cluster. Note, however, that the overlap enhancement is less pronounced, in particular in the case of triplet initial states.

It turns out that, although the spectator Ne $2p$ vacancy does not affect significantly the qualitative behavior of the interatomic decay rates, it has very strong impact on the magnitude of the widths. For example, at $R = 12$ Å, the decay width

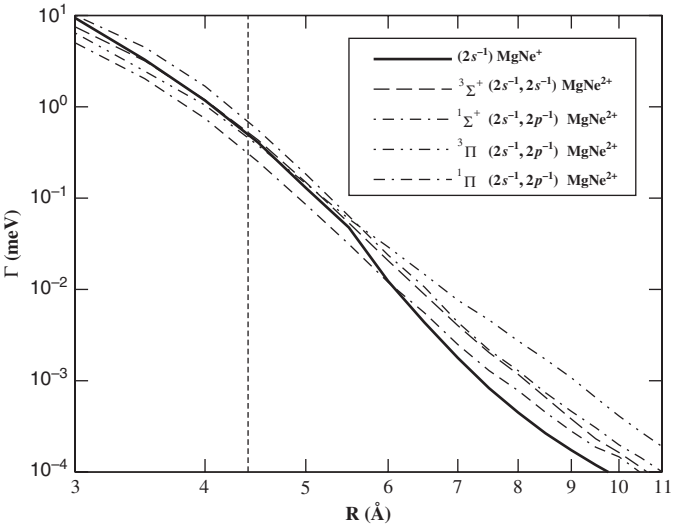

Fig. 5 Doubly logarithmic plot of the total non-radiative decay width of $MgNe^{2+}(2s^{-1}2p^{-1})$-excited state of different spatial symmetries and spin multiplicities. For reference, the *full line* shows the ICD width of the single Ne $2s$ vacancy. The equilibrium distance of MgNe in the ground state is shown by *vertical dashed line*

of the $^1\Sigma^+$ state of $MgNe^{2+}(2s^{-1}2p^{-1})$ is about 2 times larger than the width of the singly ionized cluster and the width of the $^3\Pi$ state is even 3.5 times larger. The change in the magnitude in the presence of additional vacancy is caused mainly by two factors. First, the electron missing in the $2p$ shell reduces the number of decay pathways, which increases the lifetime of the decaying state. On the other hand, spatial orbitals of multiple ionized atom or molecule are more compact, which increase their Coulombic coupling and in turn also the efficiency of the energy-transfer-dominated pathways of the interatomic decay process. The competition of these two effect explains why, at large distances where the energy-transfer character of the decay prevails, the excited doubly ionized states decay faster. In the orbital overlap-dominated region, on the other hand, the compactness of the atomic orbitals leads to reduction of the overlap enhancement, in particular for the triplet initial states.

To understand more deeply the diverse magnitudes of the total decay widths of various doubly ionized states of different spatial symmetry and spin multiplicity, particular decay pathways and corresponding partial decay widths have to be analyzed. It appears that, for the $^3\Sigma^+$ initial state in particular, the vacancy in the $2p$ shell can impede certain very important decay pathways. For a thorough discussion the reader is referred to Ref. [64].

5 Decay Widths of Inner-Shell-Excited Systems by Fano–ADC–Stieltjes Method

ADC(n) schemes for the excited states of many-electron systems can be described within the ISR approach analogously to how it was done in Sect. 3.2 for the singly ionized states. The main difference between the ADC(n) approximations for N-electron and $(N-1)$-electron systems is the necessary inclusion of the N-electron ground state into the ISR orthonormalization procedure (see Sect. 3.2), where it plays the role of zeroth excitation class. ADC(1) scheme represents the excited N-electron states in the basis of one-hole, one-particle (1h1p) intermediate states and can be shown to be related to the well-known random phase approximation (RPA) [66]. N-electron ADC(2) uses second-order perturbation theory for the correlated ground state and expands the excited states in 1h1p and 2h2p excitation classes. ADC(2) treats the 1h1p–1h1p and 1h1p–2h2p couplings in second and first order, respectively, and neglects the coupling between different 2h2p intermediate states. The extended ADC(2) scheme, or ADC(2)x, takes into account the 2h2p–2h2p interactions to first order. The details of the ISR–ADC schemes for the calculation of the excited states can be found in Ref. [67] and references therein.

As it was emphasized in Sect. 1.2.1, RICD is always accompanied by intraatomic autoionization. Practically, this means that any computational scheme for the decay widths of inner-valence-excited states in clusters must be capable of taking the intraatomic autoionization into account. Let us concentrate for the moment on the problem of computation of autoionization widths of isolated atoms within the

Fano–ADC–Stieltjes method and construct the appropriate selection scheme for the 1h1p and 2h2p ADC intermediate states. Suppose, we are interested to compute the decay rates of excited noble gas atoms (Ne, Ar, and Kr), where the excited states belong to the ms^{-1}np Rydberg series ($m = 2,\ n \geq 3$ for Ne; $m = 3,\ n \geq 4$ for Ar; $m = 4,\ n \geq 5$ for Kr) [68]. We see that, due to energy conservation, no singly excited configuration with a hole on the ms orbital or a deeper shell can represent an open decay channel. Therefore, all such configurations should be used in constructing the bound-like state Φ [see Eq. (4)]. Similar considerations can be applied to the doubly excited configurations with one or both of the holes residing on the ms or deeper lying orbitals. We offer the following mathematical formulation of these conditions. The intermediate states $\Psi_J = \hat{C}_J \Psi_0^N$ with

$$\begin{aligned} &\{\hat{C}_J\} \in \{c_a^\dagger c_k,\ \ -\varepsilon_k > -\varepsilon_{ms}\ ; \\ &c_a^\dagger c_b^\dagger c_j c_k, a < b,\, j < k,\ \ -\varepsilon_j - \varepsilon_k > -\varepsilon_{ms}\} \end{aligned} \tag{21}$$

represent closed decay channels and should be used to expand the bound component ϕ. The quantity ε_i is the HF energy of the ith orbital, or, according to the Koopmans' theorem, the first-order approximation to the respective ionization potential.

The doubly excited configurations m$p^{-2}ab$ with both holes on the outer-valence mp orbital and a, b standing for virtual orbitals of appropriate symmetry do not appear among the states in Eq. (21). In order to decide whether to include them in the expansion of Φ or not, we need to answer the following question.

Is a *spectator* resonant Auger decay possible in the systems under study?

If the answer is positive, then excited singly ionized species with two holes in an outer-shell are allowed final states and, therefore, the configurations m$p^{-2}ab$ cannot be used to expand Φ. Since *spectator* resonant Auger decay is forbidden in Ne, Ar, and Kr, we can include the configurations m$p^{-2}ab$ among those in Eq. (21). These intermediate states are used to set up an ADC(n) matrix, which is diagonalized, and one of its eigenvectors is identified as the bound-like component Φ.

Let us now consider which configurations contribute to the continuum-like part $\chi_{\beta,\varepsilon}$. It is obvious that any singly excited configuration with a hole on an orbital higher than ms represents a valid open channel. Mathematically this condition can be written as $-\varepsilon_i < -\varepsilon_{ms}$. The allowed final states are of predominantly singly excited character, which might suggest that only singly excited configurations should be used in constructing them. However, m$p^{-2}ab$ states are necessary to describe the electronic correlation in the final state. Thus, they should be included in the expansion of the final states. Since the formulation of the Fano method which we use does not call for the orthogonality between the bound and continuum parts, we proceed as follows. The singly excited configurations obeying $-\varepsilon_i < -\varepsilon_{ms}$ together with m$p^{-2}ab$ states are used to set up another ADC(n) matrix. It is diagonalized and a number of its eigenvectors having the largest weight of singly excited configurations are taken to be the continuum states $\chi_{\beta,\varepsilon}$. Using this procedure, we

improve the description of the final states while avoiding the inclusion of spurious open channels.

We applied the selection scheme described above to compute the decay rates of the excited inner-valence states in Ne, Ar, and Kr atoms by Fano–ADC–Stieltjes method [68]. For all three atoms, we calculated the decay widths Γ of the first three inner-valence-excited states, i.e., $2s^{-1}np$ ($n = 3, 4, 5, \dots$) for Ne, $3s^{-1}np$ ($n = 4, 5, 6$) states for Ar, and $4s^{-1}\mathrm{n}p$ ($n = 5, 6, 7$) for Kr. The results are shown in Tables 1, 2, and 3.

Table 1 Experimental [69] and theoretical decay widths Γ for the autoionizing $2s^{-1}\mathrm{n}p$ ($n = 3, 4, 5$) states of Ne. The results of time-dependent density functional theory in the local density approximation (TDLDA) are taken from Ref. [70]. R-matrix (RM) theoretical results are taken from Ref. [71]

	$n = 3$	$n = 4$	$n = 5$
Γ_{exp} (meV)	13 (±2)	4.5 (±1.5)	2 (±1)
$\Gamma_{\mathrm{ADC(1)}}$ (meV)	30.48	9.31	5.59
$\Gamma_{\mathrm{ADC(2)}}$ (meV)	8.93	2.86	1.72
$\Gamma_{\mathrm{ADC(2)x}}$ (meV)	11.46	3.78	1.94
Γ_{TDLDA} (meV)	13. 90	3.86	1.62
Γ_{RM} (meV)	34.9	6.65	2.47

Table 2 Experimental [72] and theoretical decay widths Γ for the autoionizing $3s^{-1}\mathrm{n}p$ ($n = 4, 5, 6$) states of Ar. The TDLDA results are taken from Ref. [70]

	$n = 4$	$n = 5$	$n = 6$
Γ_{exp} (meV)	76 (±5)	25 (±7)	16 (±7) 111
$\Gamma_{\mathrm{ADC(1)}}$ (meV)	50.61	13.52	5.59
$\Gamma_{\mathrm{ADC(2)}}$ (meV)	61.5	18.42	8.05
$\Gamma_{\mathrm{ADC(2)x}}$ (meV)	67.76	25.85	12.14
Γ_{TDLDA} (meV)	183.4	42.8	18.2

Table 3 Experimental [73] and theoretical decay widths Γ for the autoionizing $4s^{-1}\mathrm{n}p$ ($n = 5, 6, 7$) states of Kr. The TDLDA results are taken from Ref. [70]

	$n = 5$	$n = 6$	$n = 7$
Γ_{exp} (meV)	22.8 (±0.8)	13.2 (±0.5)	7.8 (±0.6)
$\Gamma_{\mathrm{ADC(1)}}$ (meV)	34.26	9.4	3.97
$\Gamma_{\mathrm{ADC(2)}}$ (meV)	42.37	12.13	5.1
$\Gamma_{\mathrm{ADC(2)x}}$ (meV)	54.69	16.14	7.16
Γ_{TDLDA} (meV)	130.4	27.8	11.6

The Fano–ADC–Stieltjes autoionization widths for inner-valence-excited states of Ne and Ar (see Tables 1 and 2) lie within the experimental error for all n's. The results in the case of Kr (Table 3) exhibit a comparatively large deviation for the lowest Rydberg term and improve greatly toward higher excitation energies. This is explained by the prevalence of electronic correlation effects in Kr which can only

partly be taken into account by the ADC(2)x technique [68]. Theoretical results obtained by TDLDA are comparable to those of Fano–ADC(2)x–Stieltjes data in the case of Ne but become worse than those for Ar and Kr. The R-matrix results, unlike the TDLDA and the present method, fail to reproduce the experimental decay width of the lowest Rydberg $2s^{-1}3p$ term in Ne.

The success of the Fano–ADC–Stieltjes method to describe the intraatomic autoionization calls for the generalization of this technique to the case of interatomic decay of inner-valence-excited states, i.e., RICD. At present, only lowest-order perturbation-theoretical (Wigner–Weisskopf) estimations of the RICD widths are available [22]. The much more accurate Fano–ADC–Stieltjes method cannot be readily applied to the RICD problem because of the full diagonalization bottleneck of the Stieltjes imaging procedure (see discussion in sect. 3.3). At present, work is in progress on the implementation of the new scheme for the Fano–ADC–Stieltjes calculation of the RICD widths.

6 Outlook

The preceding sections outlined a remarkable activity, both theoretical and experimental, aiming at in-depth study of interatomic decay processes. A manifold of new physical processes have been observed and still more new phenomena have been predicted theoretically. The first demonstration-of-principle experiment has been performed showing the potential of ICD electron spectroscopy as an analytical technique for the study of interfaces [17]. All these developments clearly point at the study of interatomic decay in clusters as at an emerging field of research. Key to theoretical progress in this new field is the ability to obtain reliable estimations of the rates of the various interatomic decay processes. The Fano–ADC–Stieltjes approach described in this chapter seems to be the method of choice. While established fairly well for singly and doubly ionized systems, the Fano–ADC–Stieltjes technique is yet to be generalized to the case of RICD of inner-valence-excited states. This goal appears to be well within reach as the full diagonalization bottleneck of the Stieltjes imaging technique has been already overcome successfully for the related problem of calculation of photoionization cross-section [57]. Furthermore, it would be desirable to extend the existing Fano–ADC–Stieltjes approaches for singly ionized states to the ADC(3) and ADC(4) levels of the ab initio theory. Indeed, going to the ADC(3) level of approximation of the many-electron states will help to describe the decay of inner-valence-ionized states more accurately than it is done on the currently implemented ADC(2)x level. This could be very important for the vacancy states of elements beyond the second row of periodic table (e.g., $3s^{-1}$ Ar^{+}). ADC(4) level of theory would provide a quantitative description of double decay processes (e.g., DICD) as well as highly accurate results for the decay of core-ionized states. As plausible applications of the envisaged ab initio theory, one could cite, for example, the rich pattern of interatomic decay processes in endohedral fullerenes. Of particular interest is the question of the relative time

scale of the various single and double decay processes as well as the possible interrelation between ultrafast character of ICD in these systems and the fullerene plasmon.

While the experiment has so far targeted rare gas clusters, a solid theoretical evidence for interatomic decay in other systems, such as hydrogen-bonded clusters and endohedral fullerenes, represents an excellent motivation for bringing some chemical diversity into the experimental studies. First steps along this direction have been taken by Hergenhahn and co-workers who have been able to measure ICD in inner-valence-ionized water clusters [74], Dörner, Jahnke, and co-workers who performed coincidence measurements on ICD in water dimer [75], and by Aziz et al. who have identified an ICD process involving a 1*s*-ionized OH^- ion and a water molecule in NaOH solution [76]. Relevance of interatomic decay processes for water and water solutions naturally leads to the question of the relevance of ICD for biochemical environment, e.g., in the processes leading to radiation damage. At present, this direction is only very little explored and certainly has a high potential for future studies.

A separate chapter in the experimental study of electronic decay has been opened with the advent of new high-frequency radiation sources: attosecond lasers [77] and X-ray free electron lasers (XFELs) [78]. Attosecond lasers operating in the XUV domain provide a unique opportunity to study the electronic decay processes in time domain using the so-called streaking probe [79]. The moderate photon energies needed to initiate interatomic decay, together with the characteristic time scales of 1–100 fs make interatomic decay processes natural candidates for the application of the attosecond pump–probe techniques. The first step toward the time-dependent theoretical description of electronic dynamics in the course of interatomic decay has been already taken [80].

While the intensities of the presently available attosecond pulses do not reach strong field regime (the laser field acting on the electrons is much weaker than the one due to atomic or molecular core), XFELs are expected to produce unprecedented field strengths of up to tens of atomic units [78]. Certainly, at such field strengths, the process of creation of a vacancy state can no longer be described perturbatively, as it is done in Sect. 2. New theoretical approaches treating the inner-shell ionization and/or excitation non-perturbatively will have to be found.

In this chapter, we have outlined the major successes and challenges of the study of interatomic decay with the particular emphasis on the development of ab initio theoretical methodology. It is our hope that more theoreticians and experimentalists will enter the new fascinating world of interatomic decay and contribute to turning the new basic concepts into a powerful spectroscopic tool.

Acknowledgments The authors would like to thank Jochen Schirmer for many fruitful discussions in the course of the work described in the present review. V. A. would like to acknowledge financial support of the Max Planck Society through the distinguished PKS postdoctoral fellowship. P. K. acknowledges financial support from the Grant GAČR 202/09/0786 of the Czech Science Foundation. Financial support of Deutsche Forschungsgemeinschaft is gratefully acknowledged.

References

1. P. Auger, J. de Phys. **6**, 205 (1925)
2. E.H.S. Burhop, W.N. Asaad, Adv. At. Mol. Phys. **8**, 163 (1972); W. Mehlhorn, *Atomic Inner-Shell Physics*, ed. by B. Crasemann (Plenum, New York, 1985)
3. N.H. Turner, J.A. Schreifels, Anal. Chem. **72**, 99R (2000)
4. C.D. Wagner, A. Joshi, J. Elec. Spectr. Rel. Phen. **47**, 283 (1988)
5. L.S. Cederbaum, J. Zobeley, F. Tarantelli, Phys. Rev. Lett. **79**, 4778 (1997)
6. R. Santra, J. Zobeley, L.S. Cederbaum, N. Moiseyev, Phys. Rev. Lett. **85**, 4490 (2000)
7. M.S. Deleuze, J.-P. Francois, E.S. Kryachko, J. Am. Chem. Soc. **127**, 16824 (2005)
8. S. Marburger, O. Kugeler, U. Hergenhahn, T. Möller, Phys. Rev. Lett. **90**, 203401 (2003)
9. T. Jahnke, A. Czasch, M.S. Schöffler, S. Schössler, A. Knapp, M. Käsz, J. Titze, C. Wimmer, K. Kreidi, R.E. Grisenti, A. Staudte, O. Jagutzki, U. Hergenhahn, H. Schmidt-Böcking, R. Dörner, Phys. Rev. Lett. **93**, 163401 (2004)
10. R. Dörner, V. Mergel, O. Jagutzki, L. Spielberger, J. Ullrich, R. Moshammer, H. Schmidt-Böcking, Physics Reports **330**, 95 (2000)
11. S. Scheit, V. Averbukh, H.-D. Meyer, N. Moiseyev, R. Santra, T. Sommerfeld, J. Zobeley, L. S. Cederbaum, J. Chem. Phys. **121**, 8393 (2004)
12. G. Öhrwall, M. Tchaplygine, M. Lundwall, R. Feifel, H. Bergersen, T. Rander, A. Lindblad, J. Schulz, S. Peredkov, S. Barth, S. Marburger, U. Hergenhahn, S. Svensson, O. Björneholm, Phys. Rev. Lett. **93**, 173401 (2004)
13. R. Santra, J. Zobeley, L.S. Cederbaum, Phys. Rev. B **64**, 245104 (2001)
14. N. Vaval, L.S. Cederbaum, J. Chem. Phys. **126**, 164110 (2007)
15. I.B. Müller, L.S. Cederbaum, J. Chem. Phys. **122**, 094305 (2005)
16. V. Averbukh, L.S. Cederbaum, Phys. Rev. Lett. **96**, 053401 (2006)
17. S. Barth, S. Marburger, S. Joshi, V. Ulrich, O. Kugeler, U. Hergenhahn, PCCP **8**, 3218 (2006)
18. S. Barth, S. Joshi, S. Marburger, V. Ulrich, A. Lindblad, G. Öhrwall, O. Björneholm, U. Hergenhahn, J. Chem. Phys. **122**, 241102 (2005)
19. T. Aoto, K. Ito, Y. Hikosaka, F. Penent, P. Lablanquie, Phys. Rev. Lett. **97**, 243401 (2006)
20. W. Eberhardt, G. Kalkoffen, C. Kunz, Phys. Rev. Lett. **41**, 156 (1978); G.C. Brown, M.H. Chen, B. Crasemann, G.E. Ice, Phys. Rev. Lett. **45**, 1937 (1980)
21. F. Gel'mukhanov, H. Ågren, Phys. Rep. **312**, 87 (1999)
22. K. Gokhberg, V. Averbukh, L.S. Cederbaum, J. Chem. Phys. **124**, 144315 (2006)
23. R. Santra, L.S. Cederbaum, Phys. Rev. Lett. **90**, 153401 (2003)
24. S. D. Stoychev, A.I. Kuleff, F. Tarantelli, L.S. Cederbaum, J. Chem. Phys. **129**, 074307 (2008)
25. Y. Morishita, X.-J. Liu, N. Saito, T. Lischke, M. Kato, G. Prümper, M. Oura, H. Yamaoka, Y. Tamenori, I.H. Suzuki, K. Ueda, Phys. Rev. Lett. **96**, 243402 (2006)
26. S.D. Stoychev, A.I. Kuleff, F. Tarantelli, L.S. Cederbaum, J. Chem. Phys. **128**, 014307 (2008)
27. K. Kreidi, T Jahnke, Th. Weber, T. Havermeier, R.E. Grisenti, X. Liu, Y. Morisita, S. Schössler, L.Ph.H. Schmidt, M. Schöffler, M. Odenweller, N. Neumann, L. Foucar, J. Titze, B. Ulrich, F. Sturm, C. Stuck, R. Wallauer, S. Voss, I. Lauter, H.K. Kim, M. Rudloff, H. Fukuzawa, G. Prümper, N. Saito, K. Ueda, A. Czasch, O. Jagutzki, H. Schmidt-Böcking, S.K. Semenov, N.A. Cherepkov, R. Dörner, J. Phys. B **41**, 101002 (2008)
28. K. Kreidi, T. Jahnke, Th. Weber, T. Havermeier, X. Liu, Y. Morisita, S. Schössler, L.Ph.H. Schmidt, M. Schöffler, M. Odenweller, N. Neumann, L. Foucar, J. Titze, B. Ulrich, F. Sturm, C. Stuck, R. Wallauer, S. Voss, I. Lauter, H.K. Kim, M. Rudloff, H. Fukuzawa, G. Prümper, N. Saito, K. Ueda, A. Czasch, O. Jagutzki, H. Schmidt-Böcking, S. Stoychev, Ph. V. Demekhin, R. Dörner, Phys. Rev. A **78**, 043422 (2008)
29. M. Yamazaki, J. Adachi, Y. Kimura, A. Yagishita, M. Stener, P. Decleva, N. Kosugi, H. Iwayama, K. Nagaya, M. Yao, Phys. Rev. Lett. **101**, 043004 (2008)
30. K. Ueda, private communication.
31. L.S. Cederbaum, F. Tarantelli, J. Chem. Phys. **98**, 9691 (1993)
32. S. Scheit, L.S. Cederbaum, H.-D. Meyer, J. Chem. Phys. **118**, 2092 (2003)

33. S. Scheit, V. Averbukh, H.-D. Meyer, J. Zobeley, L.S. Cederbaum, J. Chem. Phys. **124**, 154305 (2006)
34. U.V. Riss, H.-D. Meyer, J. Phys. B **26**, 4593 (1993)
35. J.G. Muga, J.P. Palao, B. Navarro, I.L. Egusquiza, Phys. Rep. **395**, 357 (2004)
36. R. Santra, L.S. Cederbaum, H.-D. Meyer, Chem. Phys. Lett. **303**, 413 (1999)
37. N. Moiseyev, J. Phys. B **31**, 1431 (1998); U.V. Riss, H.-D. Meyer, J. Phys. B **31**, 2279 (1998)
38. J. Schirmer, L.S. Cederbaum, O. Walter, Phys. Rev. A **28**, 1237 (1983); L.S. Cederbaum, in *Encyclopedia of Computational Chemistry*, eds. by P.v.R. Schleyer, P.R. Schreiner, N.A. Allinger, T. Clark, J. Gasteiger, P. Kollman, H.F. Schaefer III (Wiley, New York, 1998)
39. J. Schirmer, Phys. Rev. A **43**, 4647 (1991); F. Mertins, J. Schirmer, Phys. Rev. A **53**, 2140 (1996); A. B. Trofimov, J. Schirmer, J. Chem. Phys. **123**, 144115 (2005) J. Schirmer and F. Mertins, Int. J. Quant. Chem. **58**, 329 (1996).
40. R. Santra, L.S. Cederbaum, Phys. Rep. **368**, 1 (2002)
41. A.B. Trofimov, J. Schirmer, J. Chem. Phys. **123**, 144115 (2005)
42. I.B. Müller, Ph.D. thesis, Universität Heidelberg, 2006, in German
43. H. Hennig, Diploma thesis, Universität Heidelberg, 2004, in German
44. V. Averbukh, L.S. Cederbaum, J. Chem. Phys. **123**, 204107 (2005)
45. U. Fano, Phys. Rev. **124**, 1866 (1961)
46. P.W. Langhoff, in *Electron-Molecule and Photon-Molecule Collisions*, eds. by T. Rescigno, V. McKoy, B. Schneider (Plenum, New York, 1979); A. U. Hazi, *ibid.*
47. G. Howat, T. Åberg, O. Goscinski, J. Phys. B **11**, 1575 (1978)
48. T. Åberg, G. Howat, in *Handbuch der Physik*, Vol 31, ed. by W. Mehlhorn (Springer, Berlin, 1982)
49. A. Szabo, A.S. Ostlund, *Modern Quantum Chemistry: Introduction to Advanced Electronic Structure Theory* (Dover, New York, 1996)
50. J. Schirmer, A.B. Trofimov, G. Stelter, J. Chem. Phys. **109**, 4734 (1998)
51. E. Davidson, J. Comp. Phys. **17**, 87 (1975)
52. V. Averbukh, L.S. Cederbaum, J. Chem. Phys. **125**, 094107 (2006)
53. F. Müller-Plathe, G.H.F. Diercksen, in *Electronic Structure of Atoms, Molecules and Solids*, eds. by S. Canuto, J. D'Albuquerque e Castro, F.J. Paixão (World Scientific, Singapore, 1990); F. Müller-Plathe, G.H.F. Diercksen, Phys. Rev. A **40**, 696 (1989)
54. I. Cacelli, V. Caravetta, R. Moccia, Mol. Phys. **59**, 385 (1986)
55. R.K. Nesbet, Phys. Rev. A **14**, 1065 (1976)
56. K. Gokhberg, V. Visotskiy, L.S. Cederbaum, V. Averbukh, J. Chem. Phys. **130**, 064104 (2009)
57. B.N. Parlett, *The Symmetric Eigenvalue Problem* (Prentice-Hall, Englewood Cliffs, 1980)
58. J.A.D. Matthew, Y. Komninos, Surf. Sci. **63**, 716 (1975)
59. T.D. Thomas, C. Miron, K. Wiesner, P. Morin, T.X. Carroll, L.J. Sæthre, Phys. Rev. Lett. **89**, 223001 (2002)
60. D.C. Griffin, D.M. Mitnick, N.R. Randell, J. Phys. B **34**, 4401 (2001)
61. V. Averbukh, I.B. Müller, L.S. Cederbaum, Phys. Rev. Lett. **93**, 263002 (2004)
62. T.A. Carlson, M.O. Krause, Phys. Rev. Lett. **14**, 390 (1965); Phys. Rev. Lett. **17**, 1079 (1966)
63. Y. Morishita, N. Saito, I.H. Suzuki, H. Fukuzawa, X.-J. Liu, K. Sakai, G. Prümper, K. Ueda, H. Iwayama, K. Nagaya, M. Yao, K. Kreidi, M. Schöffler, T. Jahnke, S. Schössler, R. Dörner, T. Weber, J. Harries, Y. Tamenori, J. Phys. B **41**, 025101 (2008)
64. P. Kolorenč, V. Averbukh, K. Gokhberg, L.S. Cederbaum, J. Chem. Phys. **129**, 244102 (2008)
65. J. Schirmer, A. Barth, Z. Phys. A **317**, 267 (1984)
66. J. Schirmer, F. Mertins, J. Phys. B **29**, 3559 (1996)
67. J. Schirmer, A. Trofimov, J. Chem. Phys. **120**, 11449 (2004)
68. K. Gokhberg, V. Averbukh, L.S. Cederbaum, J. Chem. Phys. **126**, 154107 (2007)
69. K. Codling, R. Madden, D. Ederer, Phys. Rev. **155**, 26 (1967)
70. M. Stener, P. Decleva, A. Lisini, J. Phys. B **28**, 4973 (1995)
71. K. Schulz, M. Domke, R. Püttner, A. Gutierrez, G. Kaindl, G. Miecznik, C. Greene, Phys. Rev. A **54**, 3095 (1996)

72. S. Sorensen, T. Åberg, J. Tulkki, E. Rachlew-Kälne, G. Sundström, M. Kirm, Phys. Rev. A **50**, 1218 (1994)
73. D.L. Ederer, Phys. Rev. A **4**, 2263 (1971)
74. U. Hergenhahn, private communication.
75. T. Jahnke, R. Dörner, private communication.
76. E.F. Aziz, N. Ottoson, M. Faubel, I.V. Hertel, B. Winter, Nature **455**, 89 (2008)
77. M. Hentschel, R. Kienberger, Ch. Spielmann, G. A. Reider, N. Milosevic, T. Brabec, P. Corkum, U. Heinzmann, M. Drescher, F. Krausz, Nature **414**, 509 (2001); G. Sansone, E. Benedetti, F. Calegari, C. Vozzi, L. Avaldi, R. Flammini, L. Poletto, P. Villoresi, C. Altucci, R. Velotta, S. Stagira, S. De Silvestri, M. Nisoli, Science **314**, 443 (2006)
78. M.A. Kornberg, A.L. Godunov, S. Itza-Ortiz, D.L. Ederer, J.H. McGuire, L. Young, J. Synchrotron Rad. **9**, 298 (2002)
79. M. Drescher, M. Hentschel, R. Kienberger, M. Uiberacker, V. Yakovlev, A. Scrinzi, Th. Westerwalbesloh, U. Kleineberg, U. Heinzmann, F. Krausz, *Nature* **419**, 803 (2002)
80. A.I. Kuleff, L.S. Cederbaum, *Phys. Rev. Lett.* **98**, 083201 (2007)